

Acoustic Scattering Performance for Sources in Arbitrary Motion

Yunpeng Ma¹, Lifeng Wang^{1*} and Mingxu Yi¹

Abstract: In this paper, an analytical time domain formulation based on Ffowcs Williams-Hawkings (FW-H) equation is derived for the prediction of the acoustic velocity field generated by moving bodies. This provides the imposition of the Neumann boundary condition on a rigid scattering surface. In order to calculate the scattering sound pressure of the duct, a thin-body boundary element method (BEM) has been proposed. The radiate sound pressure is calculated using the acoustic analogy FW-H equation. The scattering effect of the duct wall on the propagation of the sound wave is presented using the thin-body BEM. Computational results for a pulsating sphere, dipole source, and a tail rotor verify the method. The sound pressure directivity and scattering effect are shown to demonstrate the applicability and validity of the approach.

Keywords: Scattering performance, Ffowcs Williams-Hawkings equation, acoustic velocity, boundary element method.

Nomenclature

n : normal vector

ρ_0 : fluid density

ω : rotational angular velocity

c_0 : sound speed

a'_{Ti} : acoustic velocity components for thickness source

a'_{Li} : acoustic velocity components for loading source

$G(x, y, t - \tau)$: Green function in time domain

$G(x, y, \omega)$: Green function in frequency domain

t : observe time

τ : emission time

p' : sound pressure in time domain

¹ School of Aeronautic Science and Technology, Beihang University, Beijing, China.

P' : sound pressure in frequency domain

P'_I : incident sound pressure in frequency domain

P'_S : sound pressure in frequency domain

x : observer position

y : source position

r : distance between observer and source

k : wave number

S : duct surface

s : imaginary surface

1 Introduction

In recent decades, noise pollution has become a major issue of concern and the noise generation mechanisms have been investigated widely. Noise generated by aircraft, fans and others has great influence on the aeroacoustic research [Huang, Zhang and Xiang et al. (2015); Qian, Han and Atluri (2013); Kingan (2014); Johnson (1980); Mao, Zhang, Xu and Qi (2015)]. In these applications, the direct sound field and scattering effect are always considered to assess the acoustic impact of sound sources.

The aerodynamic noise is based on the distinction between noise generation and propagation. The acoustic analogy and Kirchhoff method are two of the most popular noise computation method. Calculation of the acoustic field radiated by rotating sources is a meaningful problem in the prediction of noise of aircraft rotors. The main techniques for noise prediction are based on acoustic analogy Curle equation, FW-H (Ffowcs Williams-Hawkings) equation and the generalized treatment of Goldstein [Ffowcs Williams and Hawkings (1969); Farassat and Brentner (1988); Farassat and Brentner (1998)]. The inhomogeneous acoustic wave equation divides the aero-acoustic source into three types: monopole source, dipole source and quadruple source.

The ability to solve the velocity components of a sound by a solid object is one of the most important goals in aeroacoustic research. They are used to deal with scattering problems, such as noise scattering by fuselage and noise scattering in rotating machines and wings in aircraft [Mao and Qi (2009); McAlpine, Astley and Hii et al. (2006)]. To evaluate the acoustic velocity, the common method is to use the acoustic pressure gradient through the linearized momentum equation. However, the evaluation of the pressure gradient may cost a lot of computing time and storage space. Recently, Lee et al. [Lee, Brentner and Farassat et al. (2009)] have proposed an efficient formulation for computation of the pressure gradient. Ghorbaniasl et al. [Ghorbaniasl and Hirsch et al. (2015)] used it to obtain an analytical formulation for the acoustic velocity. This formulation makes it easy and convenient to solve the velocity components of a sound wave.

Since scattering sound wave may be greater amplitude than the incident sound wave, several methods have been proposed to calculate the acoustic scattering [Tausch and Xiao

(2010); Dunn and Tinetti (2008); Lee, Brentner and Morris (2010)]. The evaluation of the acoustic velocity on the scattering surface is required in order to meet the boundary conditions [Kingan, Powles and Self (2010); Swift, Blaisdell and Lyrantzis (1983)]. The acoustic boundary element method (BEM) is usually applied to predict the sound radiating and scattering field in the exterior and interior closed domain [Ciskowski and Brebbia (1991); Wu (2000)]. Wu and Wang [Wu and Wan (1992)] proposed a thin-body BEM, in which an imaginary interface is constructed to divide the domain into interior and exterior subdomains, and the imaginary surface is not discretized in the numerical implementation.

In this paper, the analytical formulation of the acoustic velocity computation is also derived for sources in arbitrary motion. In order to consider the scattering effect of the thin duct, the newly developed FW-H-Helmholtz boundary elements method is introduced. The derived velocity analytical formulation is used as the Neumann boundary condition for the thin-body BEM. This method is not only simple to operation, but also easy to implement.

The layout of this work is as follows: In Section 2, the mathematical background of sound radiation is introduced. In Section 3, the formulation to calculate acoustic velocity is derived. In Section 4, the thin-body BEM is developed. Some examples are provided to clarify the approach in Section 5. The conclusion is given in Section 6.

2 Radiated sound field

2.1 Ffowcs Williams-Hawkings equation

In 1969, Williams Ffowcs and Hawkings [Ffowcs Williams and Hawkings (1969)] used the generalized function theory to derive the sound equation of the control plane in arbitrary motion in static fluid, that is, the famous FW-H equation. The FW-H equation can offer acoustic scatterings and reflections of turbulence over a solid wall boundary with simple shape, such as an infinite half-plane, by involving an acoustic Green's function. The FW-H equation is given by

$$\left(\frac{1}{c^2} \frac{\partial}{\partial t^2} - \frac{\partial^2}{\partial x_i^2} \right) p'(x, t) = \frac{\partial}{\partial t} \{ [\rho_0 v_n + \rho(u_n - v_n)] \delta(f) \} - \frac{\partial}{\partial x_i} \{ [-P_{ij} n_j + \rho u_i (u_n - v_n)] \delta(f) \} + \frac{\partial}{\partial x_i \partial x_j} [T_{ij} H(f)] \quad (1)$$

for inviscid flow, $\frac{1}{c^2} \frac{\partial}{\partial t^2} - \frac{\partial^2}{\partial x_i^2}$ is wave operator, u_i is velocity, f denotes a moving

Kirchhoff surface, p' is acoustic pressure, v_n is normal component of surface velocity. P_{ij} denotes the compressive stress tensor, $T_{ij} = -P'_{ij} + \rho u_i u_j - c^2 \rho' \delta_{ij}$ denotes a component of the Lighthill tensor, $\delta(f)$ is Dirac delta function, $H(f)$ is Heaviside function and satisfied.

$$H(f) = \begin{cases} 1 & f(x_i, t) > 0 \\ 0 & f(x_i, t) < 0 \end{cases}, \delta(f) = \frac{\partial H(f)}{\partial f} \quad (2)$$

As $f(x_i, t) = 0$, according to non-penetration condition, $u_n = v_n$, FW-H equation can be reduced as below

$$\left(\frac{1}{c^2} \frac{\partial}{\partial t^2} - \frac{\partial^2}{\partial x_i^2} \right) p'(x, t) = \frac{\partial}{\partial t} [\rho_0 v_n \delta(f)] - \frac{\partial}{\partial x_i} [P_{ij} n_j \delta(f)] + \frac{\partial}{\partial x_i \partial x_j} [T_{ij} H(f)] \quad (3)$$

$\partial[\rho_0 v_n \delta(f)]/\partial t$, $-\partial[P_{ij} n_j \delta(f)]/\partial x_i$ and $\partial^2 [T_{ij} H(f)]/\partial x_i \partial x_j$ are monopole source, dipole source and quadruple source, respectively. According to Hanson and Fink's theory [Farassat (2007)]. Eq. (3) can be simplified to

$$\left(\frac{1}{c^2} \frac{\partial}{\partial t^2} - \frac{\partial^2}{\partial x_i^2} \right) p'(x, t) = \frac{\partial}{\partial t} [\rho_0 v_n \delta(f)] - \frac{\partial}{\partial x_i} [P_{ij} n_j \delta(f)] \quad (4)$$

2.2 Farassat method

From the end of 1970s to the beginning of 1980s, basing on the integral of Green Function, conversion of the spatial derivatives and time derivatives, Farassat published the famous Farassat 1 and Farassat 1A formulations which are the solution of time domain integral expressions for the thickness noise and loading noise of FW-H equation. The solution of Eq. (4), the formulation of Farassat 1A, is expressed as follows [Dunn, Tinetti and Nark (2015)]

$$p'(x, t) = p'_T(x, t) + p'_L(x, t) \quad (5)$$

with

$$4\pi p'_T(x, t) = \int_S \left[\frac{\rho_0 \dot{v}_n}{r(1-M_r)^2} \right]_{ret} dS + \int_S \left[\frac{\rho_0 v_n (r \dot{M}_i \hat{r}_i + c_0 M_r - c_0 M^2)}{r^2 (1-M_r)^3} \right]_{ret} dS \quad (6)$$

$$4\pi p'_L(x, t) = \frac{1}{c_0} \int_S \left[\frac{\dot{l}_i \hat{r}_i}{r(1-M_r)^2} \right]_{ret} dS + \int_S \left[\frac{l_r - l_i M_i}{r^2 (1-M_r)^2} \right]_{ret} dS \quad (7)$$

$$+ \frac{1}{c_0} \int_S \left[\frac{l_r (r \dot{M}_i \hat{r}_i + c_0 M_r - c_0 M^2)}{r^2 (1-M_r)^3} \right]_{ret} dS$$

$p'_T(x, t)$ is thickness noise and $p'_L(x, t)$ is loading noise. The subscript *ret* indicates that all of the values have to be taken at the retarded time. The dot over the quantity denotes the differentiation of this magnitude with respect to the emission time.

3 Acoustic velocity formulation for sources in arbitrary motion

The procedure of the velocity formulation for the thickness and loading sources has been

recently proposed by [Farassat (2007)]. Following the same procedure gives the thickness and loading acoustic velocity as follows:

$$4\pi\rho_0 a'_{Ti}(x, t) = -\int_S \frac{\partial}{\partial x_i} \left[\frac{Q}{r(1-M_r)} \right]_{ret} dS \quad (8)$$

$$4\pi\rho_0 a'_{Li}(x, t) = -\frac{1}{c_0} \int_S \frac{\partial}{\partial x_i} \left[\frac{L_r}{r(1-M_r)} \right]_{ret} dS - \int_0^t \left(\int_S \frac{\partial}{\partial x_i} \left[\frac{L_r}{r^2(1-M_r)} \right]_{ret^*} dS \right) dt^* \quad (9)$$

where $Q = \rho(u_n - v_n) + \rho_0 v_n$, a'_{Ti} and a'_{Li} are the acoustic velocity components for the thickness and loading sources. u_n and v_n are the fluid and the data surface normal velocity, respectively. ρ denotes the local fluid density, and ρ_0 is the density of the undisturbed medium. The subscript ret^* indicates that all of the values have to be taken at the retarded time t^* .

For any function $F(x, \tau(x, t))$, one has

$$\left. \frac{\partial F}{\partial x_i} \right|_t = \left. \frac{\partial F}{\partial x_i} \right|_\tau + \left. \frac{\partial F}{\partial \tau} \right|_x \left. \frac{\partial \tau}{\partial x_i} \right|_t \quad (10)$$

Using Eq. (10) and $\left. \frac{\partial \tau}{\partial t} \right|_x = \left[\frac{1}{(1-M_r)} \right]_{ret}$, we can obtain the velocity formulation V1 for the thickness and loading sources, respectively.

$$4\pi\rho_0 a'_{Ti}(x, t) = \frac{1}{c_0} \frac{\partial}{\partial t} \int_S \left[\frac{Q \hat{r}_i}{r(1-M_r)} \right]_{ret} dS + \int_S \left[\frac{Q \hat{r}_i}{r^2(1-M_r)} \right]_{ret} dS \quad (11)$$

$$4\pi\rho_0 a'_{Li}(x, t) = \frac{1}{c_0^2} \frac{\partial}{\partial t} \int_S \left[\frac{\hat{r}_i L_r}{r(1-M_r)} \right]_{ret} dS - \frac{1}{c_0} \int_S \left[\frac{L_i - 3\hat{r}_i L_r}{r^2(1-M_r)} \right]_{ret} dS - \int_0^t \left(\int_S \left[\frac{L_i - 3\hat{r}_i L_r}{r^3(1-M_r)} \right]_{ret^*} dS \right) dt^* \quad (12)$$

To improve the speed and accuracy of the velocity formulation V1, the time derivatives of formulation V1 can be taken inside the integrals. From the Eq. (11), one obtains

$$\frac{\partial}{\partial t} \int_S \left[\frac{Q \hat{r}_i}{r(1-M_r)} \right]_{ret} dS = \int_S \left[\hat{r}_i \frac{\partial}{\partial t} \left(\frac{Q}{r(1-M_r)} \right) \right]_{ret} dS + \int_S \left[\frac{Q}{r(1-M_r)} \frac{\partial \hat{r}_i}{\partial t} \right]_{ret} dS \quad (13)$$

Since

$$\left. \frac{\partial(\hat{r}_i)}{\partial t} \right|_x = \left[\frac{1}{r(1-M_r)} \right]_{ret} \left. \frac{\partial(\hat{r}_i)}{\partial \tau_{ret}} \right|_x - \left[\frac{r_i}{r^2(1-M_r)} \right]_{ret} \left. \frac{\partial r_{ret}}{\partial \tau_{ret}} \right|_x = \left[\frac{-c_0 M_i + c_0 \hat{r}_i M_r}{r(1-M_r)} \right]_{ret} \quad (14)$$

The second term of the right hand of Eq. (13) can be given by

$$\int_S \left[\frac{Q}{r(1-M_r)} \frac{\partial \hat{r}_i}{\partial t} \right]_{ret} dS = c_0 \int_S \left[Q \frac{M_r \hat{r}_i - M_i}{r^2(1-M_r)^2} \right]_{ret} dS \quad (15)$$

Then Eq. (11) becomes

$$4\pi\rho_0 a'_{Ti}(x,t) = \frac{1}{c_0} \int_S \left[\hat{r}_i \frac{\partial}{\partial t} \left(\frac{Q}{r(1-M_r)} \right) \right]_{ret} dS + \int_S \left[Q \frac{M_r \hat{r}_i - M_i}{r^2(1-M_r)^2} \right]_{ret} dS + \int_S \left[\frac{Q \hat{r}_i}{r^2(1-M_r)} \right]_{ret} dS \quad (16)$$

or

$$4\pi\rho_0 a'_{Ti}(x,t) = \frac{1}{c_0} \int_S \left[\hat{r}_i \frac{\partial}{\partial t} \left(\frac{Q}{r(1-M_r)} \right) \right]_{ret} dS - \int_S \left[Q \frac{M_i - \hat{r}_i}{r^2(1-M_r)^2} \right]_{ret} dS \quad (17)$$

Let

$$I_T = \frac{\partial}{\partial t} \left[\frac{Q}{r(1-M_r)} \right] = \frac{1}{1-M_r} \frac{\partial}{\partial \tau} \left[\frac{Q}{r(1-M_r)} \right] \quad (18)$$

Expansion of the expression in the same manner as in the derivation of Farassat 1A gives

$$I_T = \frac{\dot{Q}}{r(1-M_r)^2} + Q \frac{r\dot{M}_r + c_0(M_r - M^2)}{r^2(1-M_r)^3} \quad (19)$$

where $\dot{M}_r = \dot{M}_i \hat{r}_i$. Then the acoustic velocity components for the thickness sources are got

$$4\pi\rho_0 a'_{Ti}(x,t) = \frac{1}{c_0} \int_S \left[\hat{r}_i I_T \right]_{ret} dS - \int_S \left[Q \frac{M_i - \hat{r}_i}{r^2(1-M_r)^2} \right]_{ret} dS \quad (20)$$

Next, simplifying Eq. (12) further, one can rewrite it as follows

$$4\pi\rho_0 a'_{Li}(x,t) = \frac{1}{c_0} \int_S \hat{r}_i \frac{\partial}{\partial t} \left[\frac{L_r}{r(1-M_r)} \right]_{ret} dS + \frac{1}{c_0^2} \int_S \left[\frac{L_r}{r(1-M_r)} \frac{\partial \hat{r}_i}{\partial t} \right]_{ret} dS - \frac{1}{c_0} \int_S \left[\frac{L_i - 3\hat{r}_i L_r}{r^2(1-M_r)} \right]_{ret} dS - \int_0^t \left(\int_S \left[\frac{L_i - 3\hat{r}_i L_r}{r^3(1-M_r)} \right]_{ret} dS \right) dt^* \quad (21)$$

Using Eq. (14), we have

$$4\pi\rho_0 a'_{Li}(x, t) = \frac{1}{c_0} \int_S \left[\hat{r}_i \left(\frac{1}{c_0} \frac{\partial}{\partial t} \left[\frac{L_r}{r(1-M_r)} \right]_e + \left[\frac{L_r}{r^2(1-M_r)} \right] \right) \right]_{ret} dS - \frac{1}{c_0} \int_S \left[L_r \frac{M_i - \hat{r}_i}{r^2(1-M_r)^2} \right]_{ret} dS - \frac{1}{c_0} \int_S \left[\frac{L_i - L_r \hat{r}_i}{r^2(1-M_r)} \right]_{ret} dS - \int_0^t \left(\int_S \left[\frac{L_i - 3\hat{r}_i L_r}{r^3(1-M_r)} \right]_{ret^*} dS \right) dt^* \quad (22)$$

Let

$$I_L = \frac{1}{c_0} \frac{\partial}{\partial t} \left[\frac{L_r}{r(1-M_r)} \right]_e + \left[\frac{L_r}{r^2(1-M_r)} \right] \quad (23)$$

Expansion of the expression in the same manner as in the derivation of Farassat 1A gives

$$I_L = \frac{1}{c_0} \frac{L_r}{r(1-M_r)^2} + \frac{L_r - L_M}{r^2(1-M_r)^2} + \frac{1}{c_0} L_r \frac{r\dot{M}_r + c_0(M_r - M^2)}{r^3(1-M_r)^3} \quad (24)$$

where $\dot{L}_r = \dot{L}_i \hat{r}_i$, $L_M = L_i M_i$. Finally, the acoustic velocity components for the loading sources are obtained as follows

$$4\pi\rho_0 a'_{Li}(x, t) = \frac{1}{c_0} \int_S [\hat{r}_i I_L]_{ret} dS - \frac{1}{c_0} \int_S \left[L_r \frac{M_i - \hat{r}_i}{r^2(1-M_r)^2} \right]_{ret} dS - \frac{1}{c_0} \int_S \left[\frac{L_i - \hat{r}_i L_r}{r^2(1-M_r)} \right]_{ret} dS - \int_0^t \left(\int_S \left[\frac{L_i - 3\hat{r}_i L_r}{r^3(1-M_r)} \right]_{ret^*} dS \right) dt^* \quad (25)$$

4 Thin-body acoustic boundary element method (BEM)

In this section, a thin-body boundary integral formulation is applied to calculate the far field sound pressure. Due to the scattering effect of the solid wall in the duct, the total sound pressure is acquired as the sum of the incident and scattered pressure

$$P'(x, \omega) = P'_i(x, \omega) + P'_s(x, \omega) \quad (26)$$

where P'_i and P'_s are incident and scattered sound pressure in the frequency domain, respectively. The incident sound pressure can be obtained by using Eq. (6), Eq. (7), and they were transformed into data in frequency domain by using Fast Fourier Transform (FFT) method. The scattered sound pressure will be got by using BEM. The calculated domain is shown in Figure 1, the surface of the duct is denoted as S , an imaginary surface s is added to close the duct and divide the computational domain into an interior subdomain D^+ and an exterior subdomain D^- . The sound pressure on the outside of the surface $S + s$ is denoted by P'^- and that on the inside is denoted by P'^+ . The integral

equation can be used to each subdomain [Wu and Wan (1992)]

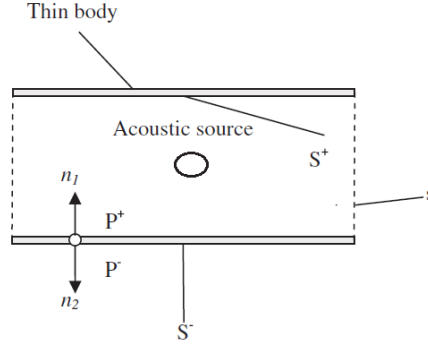


Figure 1: A diagram of acoustic scattering by a thin-body.

$$C^+(x)P'^+(x, \omega) = P'_l(x, \omega) + \int_{S+S^+} \left[\frac{\partial P'^+(y, \omega)}{\partial n_1(y)} G(x, y, \omega) - P'^+(y, \omega) \frac{\partial G(x, y, \omega)}{\partial n_1(y)} \right] dS(y) \quad (27)$$

$$C^-(x)P'^-(x, \omega) = \int_{S+S^-} \left[\frac{\partial P'^-(y, \omega)}{\partial n_2(y)} G(x, y, \omega) - P'^-(y, \omega) \frac{\partial G(x, y, \omega)}{\partial n_2(y)} \right] dS(y) \quad (28)$$

where n_1 and n_2 are normal unit vectors at the two sides of the wall, $C^+(x)$ and $C^-(x)$ are the two constants that depend on the position of x

$$C^+(x) = \begin{cases} 0, & x \in D^- \\ 1, & x \in D^+ \\ 1/2, & x \in S \end{cases} \quad (29)$$

$$C^-(x) = \begin{cases} 0, & x \in D^+ \\ 1, & x \in D^- \\ 1/2, & x \in S \end{cases} \quad (30)$$

Adding Eq. (27) and Eq. (28) gives the thin-body boundary integral equation

$$\frac{1}{2}[P'^+(x, \omega) + P'^-(x, \omega)] = P'_l(x, \omega) + \int_S \left\{ G(x, y, \omega) \left[\frac{\partial P'^+(y, \omega)}{\partial n(y)} - \frac{\partial P'^-(y, \omega)}{\partial n(y)} \right] - \frac{\partial G(x, y, \omega)}{\partial n(y)} [P'^+(y, \omega) - P'^-(y, \omega)] \right\} dS(y), \quad x \in S \quad (31)$$

$$P'(x, \omega) = P'_l(x, \omega) + \int_s \left\{ G(x, y, \omega) \left[\frac{\partial P'^+(y, \omega)}{\partial n(y)} - \frac{\partial P'^-(y, \omega)}{\partial n(y)} \right] - \frac{\partial G(x, y, \omega)}{\partial n(y)} [P'^+(y, \omega) - P'^-(y, \omega)] \right\} dS(y), \quad x \in D^+ \cup D^- \cup s \quad (32)$$

where $\partial / \partial n_1 = -\partial / \partial n_2 = \partial / \partial n$, and the continuous boundary conditions of the pressure and its partial derivation on the imaginary surface s are used

$$P'^+(x, \omega) = P'^-(x, \omega), \quad \frac{\partial P'^+(x, \omega)}{\partial n(x)} = \frac{\partial P'^-(x, \omega)}{\partial n(x)}, \quad x \in s \quad (33)$$

The assumption of acoustic rigid boundary conditions is used over the entire surface S

$$\frac{\partial P'^+(x, \omega)}{\partial n(x)} = \frac{\partial P'^-(x, \omega)}{\partial n(x)} = 0, \quad x \in S \quad (34)$$

Then Eq. (31) and Eq. (32) reduce to

$$\frac{1}{2} [P'^+(x, \omega) + P'^-(x, \omega)] = P'_l(x, \omega) - \int_s \left\{ \frac{\partial G(x, y, \omega)}{\partial n(y)} [P'^+(y, \omega) - P'^-(y, \omega)] \right\} dS(y), \quad x \in S \quad (35)$$

$$P'(x, \omega) = P'_l(x, \omega) - \int_s \left\{ \frac{\partial G(x, y, \omega)}{\partial n(y)} [P'^+(y, \omega) - P'^-(y, \omega)] \right\} dS(y), \quad x \in D^+ \cup D^- \cup s \quad (36)$$

Eq. (36) is not sufficient to obtain the two unknowns $P'^+(x, \omega)$ and $P'^-(x, \omega)$. Differentiating Eq. (35) with regard to the direction of normal vector $n(x)$, it can be transformed into

$$0 = \frac{\partial P'_l(x, \omega)}{\partial n(x)} - \int_s \left\{ \frac{\partial^2 G(x, y, \omega)}{\partial n(y) \partial n(x)} [P'^+(y, \omega) - P'^-(y, \omega)] \right\} dS(y), \quad x \in S \quad (37)$$

The problem of scattering by the duct can be dealt with initially solving Eq. (37) to calculate the sound pressure jump $P'^+(y, \omega) - P'^-(y, \omega)$ on the surface S , and afterwards evaluating the acoustic pressure at any filed point. Then the acoustic pressure on both sides of the duct could be easily got. However, the value of $\frac{\partial P'_l(x, \omega)}{\partial n(x)}$ cannot be

obtained easily by using Eq. (6) or Eq. (7). We can acquire it indirectly by using the acoustic velocity formulation. If Eq. (37) satisfies the Neumann boundary condition, we will

$$\frac{\partial P'_l(x, \omega)}{\partial n(x)} = -i\omega\rho_0 v_n(x, \omega) \quad (38)$$

where $v_n = \{a'_{T1}(x, \omega), a'_{T2}(x, \omega), a'_{T3}(x, \omega)\}$ for the thickness sources,

$v_n = \{a'_{L1}(x, \omega), a'_{L2}(x, \omega), a'_{L3}(x, \omega)\}$ for the loading sources.

Then, to solve the Eq. (37), a discretized scheme based on BEM should be used to calculate the unknown value $P'^+(y, \omega) - P'^-(y, \omega)$. The simplest constant boundary element is applied in this paper and the thin-body surface S is discretized into N elements. Each element has one node which is located in the center of the element. Then, Eq. (37) can be transformed into a system of algebraic equations.

$$\phi_i = \sum_{j=1}^N (A_j \cdot dS_j) \cdot \varphi_j = \sum_{j=1}^N B_j \cdot \varphi_j, \quad (i = 1, \dots, N) \quad (39)$$

where $\phi_i = -i\omega\rho_0 v_n(x_i, \omega)$, $A_j = \frac{\partial^2 G(x_i, y_j, \omega)}{\partial n(y_j) \partial n(x_i)}$ and $\varphi_j = P'^+(y_j, \omega) - P'^-(y_j, \omega)$,

x_i and y_j are the center of element i, j , respectively. dS_j is the area of the element j .

Therefore, the form of matrix of Eq. (39) is written as

$$[\phi]^T = [B][\varphi]^T \quad (40)$$

Eq. (40) may be solved easily by using the software Mathematica. When the unknown φ is calculated, the acoustic pressure at any filed point can be obtained through Eq. (35) and (36).

The function $G(x, y, \omega)$ and its derivations $\frac{\partial G(x, y, \omega)}{\partial n(y)}$, $\frac{\partial^2 G(x, y, \omega)}{\partial n(x) \partial n(y)}$ in above equations are expressed as follows:

$$G(x, y, \omega) = \frac{e^{jkr}}{4\pi r} \quad (41)$$

$$\frac{\partial G(x, y, \omega)}{\partial n(y)} = -\left(jk + \frac{1}{r}\right) \frac{e^{jkr}}{4\pi r} \frac{\partial r}{\partial n(y)} \quad (42)$$

$$\frac{\partial^2 G(x, y, \omega)}{\partial n(x) \partial n(y)} = \frac{e^{jkr}}{4\pi r^3} [(-2 + 2jkr + k^2 r^2)] \times n(x) \cdot n(y) \quad (43)$$

5 Numerical results

In this part, the acoustic velocity field simulated by the derived formulation and scattering effect of the duct are validated through three test cases. The first case considers a monopole source, which is identified with a pulsating sphere. The second test case is a

dipole source. The third case contains the consistency test known as the Isom thickness noise. All these sources are located at the center of the duct. Showing the validity and reliability of the developed formulation for acoustic scattering problems is our main work. The sound pressure is expressed as dB (decibels) and the predicted SPLs (sound pressure levels) is given by the following

$$SPLs = 20 \lg \frac{P_e}{P_r} \tag{44}$$

where P_e denotes predicted pressure, P_r denotes the reference pressure and equals to 2×10^{-5} Pa.

5.1 Pulsating sphere

In order to verify the algorithms, the analytical solution of a monopole source has been investigated. The monopole is identified with a pulsating sphere as the small sphere with a radius a in Figure 2. The pressure fluctuation induced by the pulsating sphere is expressed by a harmonic spherical wave

$$p' = \frac{A\omega\rho_0}{4\pi r} \frac{1}{\sqrt{1+(ka)^2}} \cos[\omega t - k(r-a) + \phi_0] \tag{45}$$

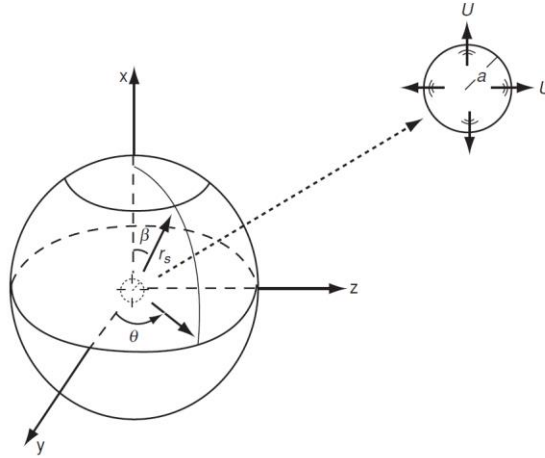


Figure 2: Monopole source and data surface are shown.

where ω and k are angular velocity and the wave number, respectively, and

$$\phi_0 = \tan^{-1}\left(\frac{1}{ka}\right), \quad r = \sqrt{x^2 + y^2 + z^2} \tag{46}$$

The velocity is given by

$$\begin{aligned}
u_r(r,t) &= \frac{1}{\rho_0} \int \frac{\partial p'}{\partial r} dt \\
&= \frac{1}{\sqrt{1+(ka)^2}} \left(\frac{Ak}{4\pi r} \cos[\omega t - k(r-a) + \varphi_0] \right. \\
&\quad \left. + \frac{A}{4\pi r^2} \sin[\omega t - k(r-a) + \varphi_0] \right)
\end{aligned} \tag{47}$$

where $A = 4\pi a^2 U$. To perform this case, we take the radius of the spherical penetrable data surface r_s to be $3.25 a$. The speed of sound c_0 is 340m/s. The density for medium is 1.2kg/m^3 . The angular velocity of the source is 1020rad/s. The other parameters are $a = 0.01\text{m}$ and $U = 8\text{m/s}$. The pulsating sphere is located at the center of the duct, which is shown in Figure 3. The diameter of the duct is 0.07m. The length of the duct is 0.5m. The observer distance is assumed to be 2m.

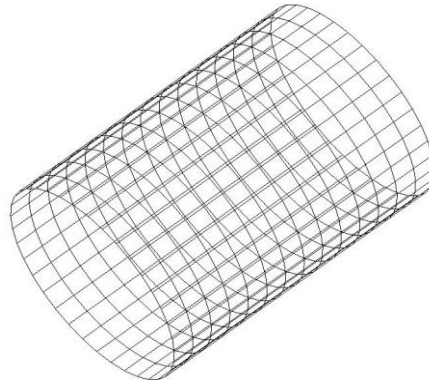


Figure 3: The duct in BEM.

The acoustic velocity components are calculated by using the numerical method. The results are compared with analytical solutions for different observer time. The x , y and z components of the acoustic velocity obtained with the derived formulation is plotted in Figures 4-6. From Figures 4-6, we find that the numerical solutions are very good agreement with the analytical solution. To perform the acoustic scattering problems of the duct, we use the thin-body BEM. Figure 7 shows the scattering performance of the pulsating sphere. The left is the incident sound pressure, the middle is the scattering effect of the duct and the right is the total sound pressure.

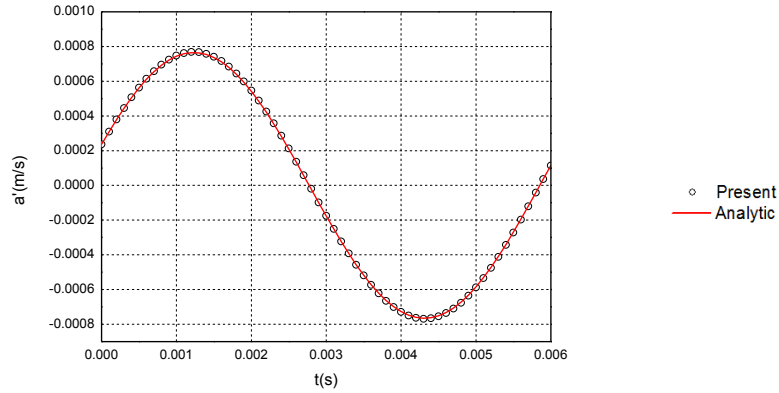


Figure 4: The calculated x -component of acoustic velocity compared with that of the analytical solution for $\beta_1 = 18^\circ$. Monopole source.

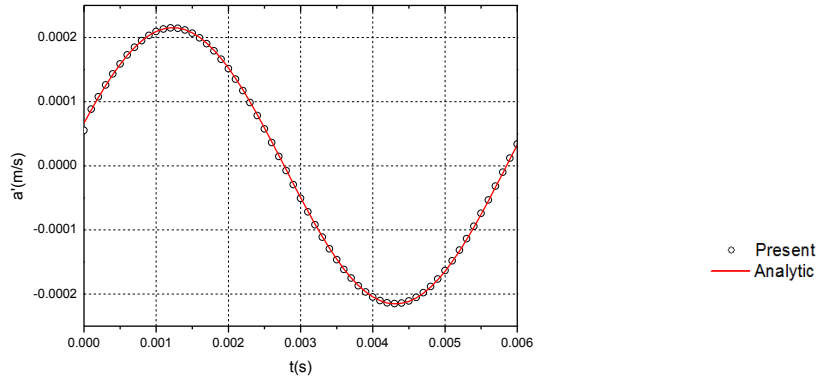


Figure 5: The calculated y -component of acoustic velocity compared with that of the analytical solution for $\beta_1 = 18^\circ$. Monopole source.

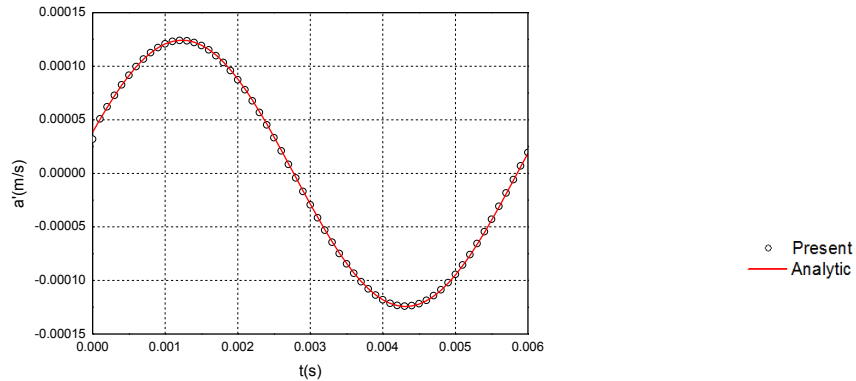


Figure 6: The calculated z -component of acoustic velocity compared with that of the

analytical solution for $\beta_1 = 18^\circ$. Monopole source.

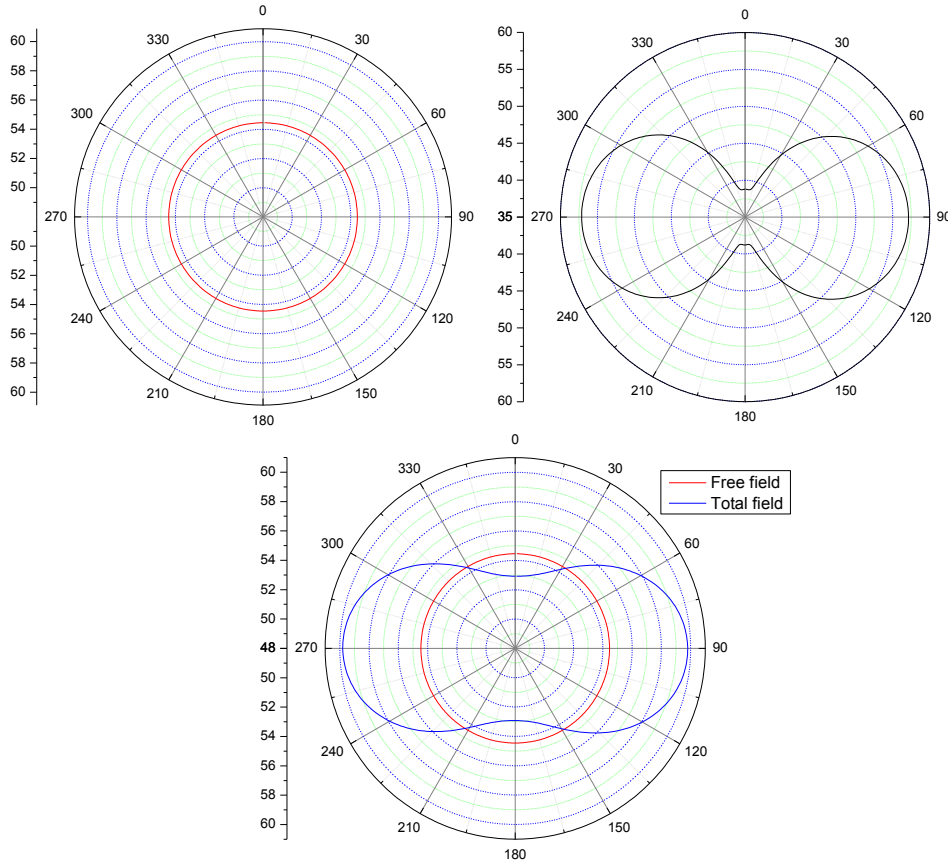


Figure 7: Directivity of calculated far-field SPLs at 4918 Hz (a) free field, (b) scattering effect of the duct and (c) total field. Monopole source.

From the Figure 7, we can see the directivity of the incident sound pressure is circular as the property of monopole sound source. When the scattering effect is considered, the directivity of the sum sound becomes non-circular. For the angle (210 to 330 degrees and 30 to 150 degrees), SPLs of the total field is louder due to scattering where at the angle (-30 to 30 degrees and 150 to 210 degrees), it is quieter. It shows that the sound pressure is strengthened in the direction of duct both ends, and the sound pressure is subdued in the other direction.

5.2 A three dimensional dipole source

A dipole point source is equivalent to a compact oscillating sphere, which is denoted as two closely positioned identical monopole point sources. A dipole has an axis, which is the line connecting the centers of the two monopoles (pulsating sphere with radius of a). The monopoles are positioned in the z direction at a distance of $d = 2.5 a$ from the center

(d is the distance between the two monopole points). The pressure fluctuation induced by the dipole source for an observer positioned at (x, y, z) is

$$p' = \frac{A\omega\rho_0}{4\pi r_1} \frac{1}{\sqrt{1+(ka)^2}} \cos[\omega t - k(r_1 - a) + \phi_0] + \frac{A\omega\rho_0}{4\pi r_2} \frac{1}{\sqrt{1+(ka)^2}} \cos[\omega t - k(r_2 - a) + \phi_0] \quad (48)$$

where

$$r_1 = \sqrt{x^2 + y^2 + (z + 0.5d)^2}, \quad r_2 = \sqrt{x^2 + y^2 + (z - 0.5d)^2} \quad (49)$$

The integration surface used in the previous test case is also used here ($r_s = 3.25a$, in Figure 8). The other parameters are the same as the previous case. The observer distance is assumed to be 5m.

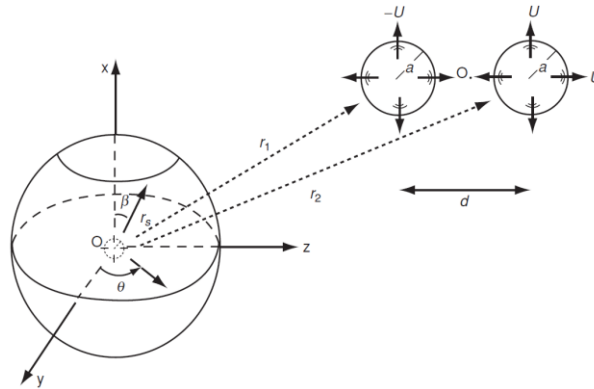


Figure 8: Dipole source and data surface are shown.

The calculation is performed for this case, and the acoustic velocity components are computed. The numerical results are compared with those of the analytical solution in Figures 9-11. Again, the numerical solution is in perfect coincidence with the analytical solution.

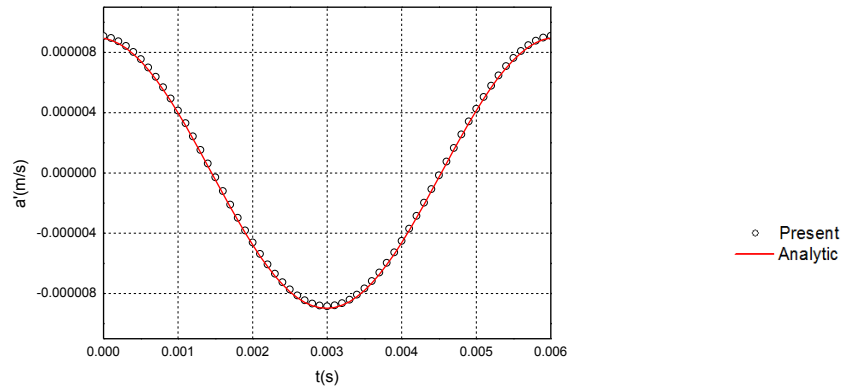


Figure 9: The calculated x -component of acoustic velocity compared with that of the analytical solution for $\beta_1 = 18^\circ$. Dipole source.

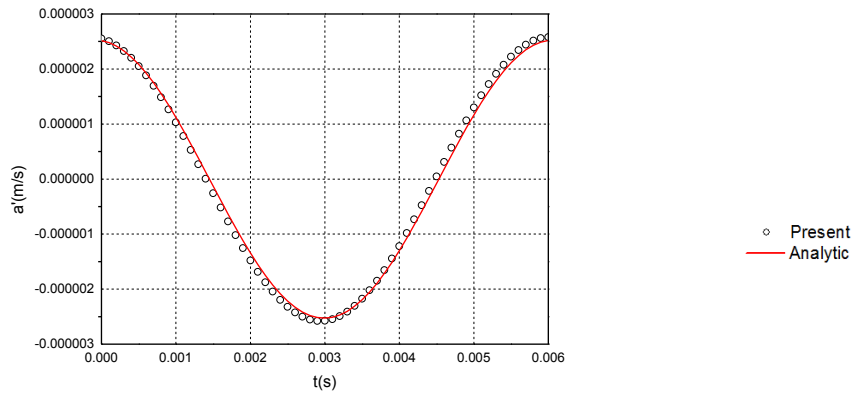


Figure 10: The calculated y -component of acoustic velocity compared with that of the analytical solution for $\beta_1 = 18^\circ$. Dipole source.

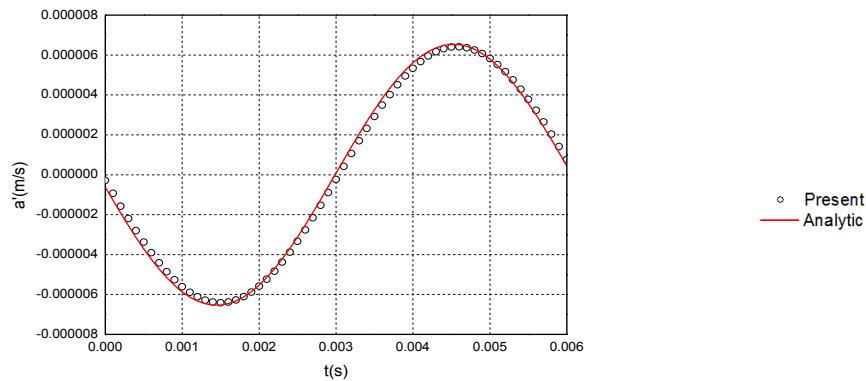


Figure 11: The calculated z -component of acoustic velocity compared with that of the analytical solution for $\beta_1 = 18^\circ$. Dipole source.

Figure 12 shows the scattering performance of the dipole source. The left is the incident sound pressure, the middle is the scattering effect of the duct and the right is the total sound pressure.

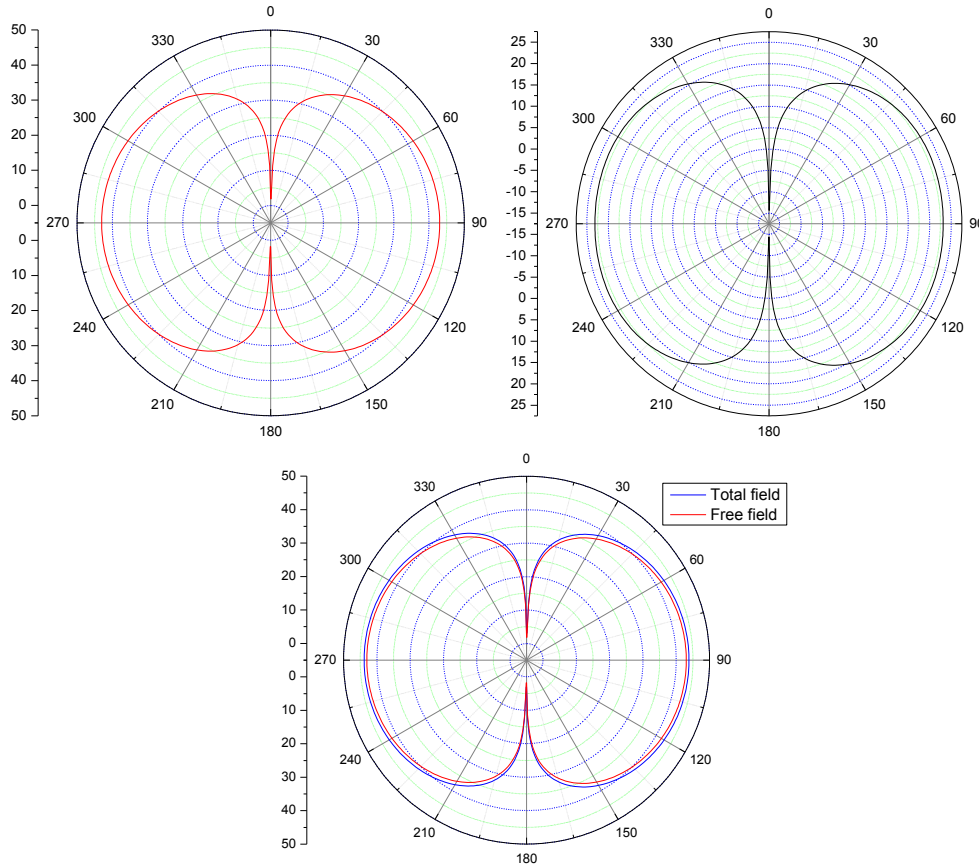


Figure 12: Directivity of calculated far-field SPLs at 4918 Hz (a) free field, (b) scattering effect of the duct and (c) total field. Dipole source.

From the Figure 12, we can find the directivity of the incident sound pressure is symmetrical as the property of dipole sound source. When the scattering effect is considered, the SPLs of the total field becomes slightly louder. It implies that the sound pressure of dipole source is strengthened through the duct scattering effect. The directivity of the total sound pressure is the same as the incident sound pressure.

5.3 Isom noise consistency

The Isom thickness noise property is discussed in [Brentner and Farassat (2003)]. When a constant aerodynamic load $p = \rho_0 c_0^2$ is used over a moving surface, the generated dipole loading noise should be identical to the monopole thickness noise. So, we only consider the dipole loading noise for this problem.

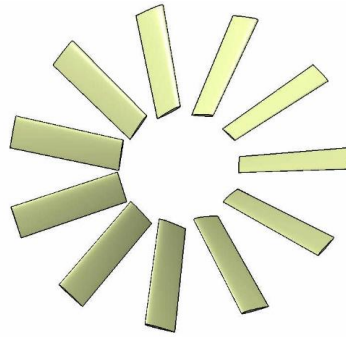


Figure 13: Geometric model of tail rotor.

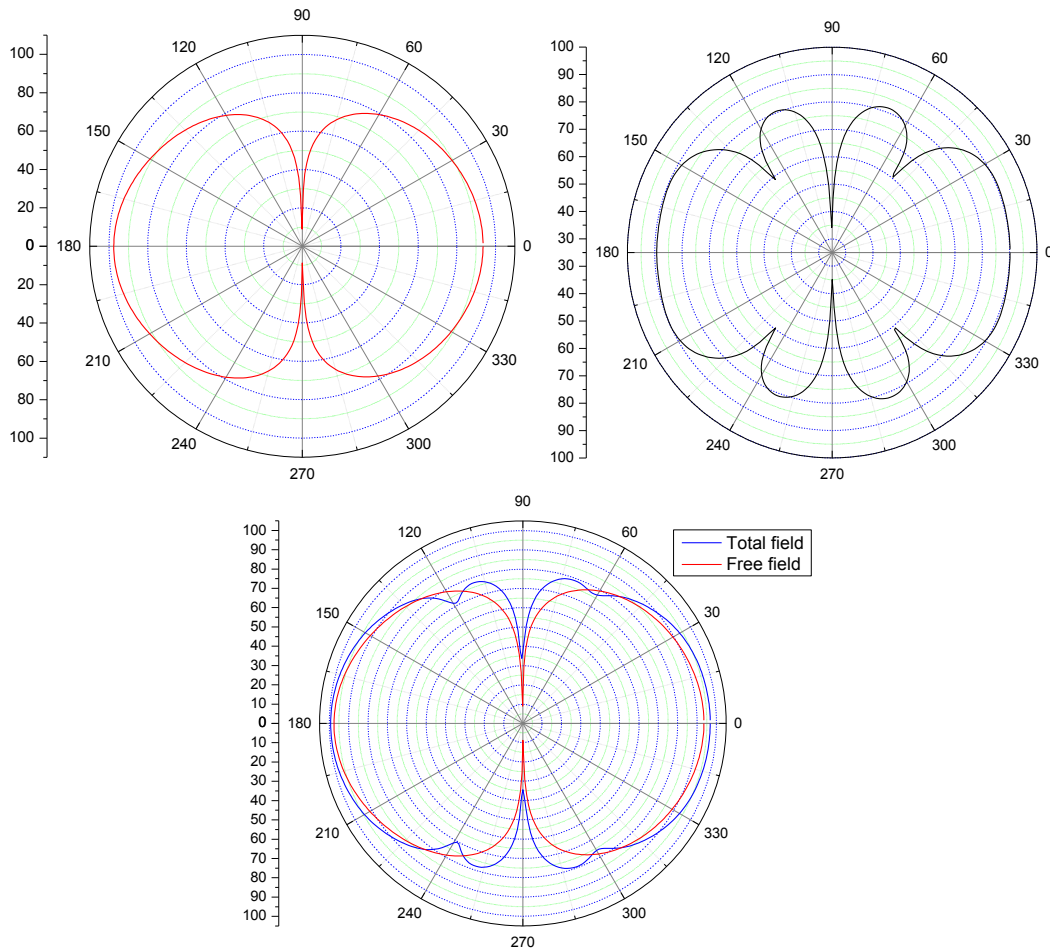


Figure 14: Directivity of calculated far-field SPLs at 4930 Hz (a) free field, (b) scattering effect of the duct and (c) total field. Isom noise source.

In this case, we will show the scattering effect of the Isom noise consistency. The numerical example is applied to the noise generated by the flow around a helicopter tail

rotor. The tail rotor consists of 11 equally spaced blades 0.594m in diameter with a constant chord of 0.056m. The CATIA geometric model of the tail rotor is shown in Figure 13. The blade tip Mach number is 0.8. The tail rotor is located at the center of the duct with diameter 0.7m, and length 1.5m. The observer is located 5m from the origin of the blade fixed frame.

The incident sound pressure, the scattering sound pressure and the total sound pressure generated by the Isom source are shown in Figure 14.

From the Figure 14, we can conclude the directivity of incident sound pressure and total sound pressure are the similar to the dipole noise source. The total sound pressure of Isom noise source is strengthened due to the duct scattering effect of the duct. However, the total sound pressure is slightly quieter in some local direction. The reason for the sound decreasing is likely due to noise cancellation.

6 Conclusion

The aim of this paper is to develop the FW-H/thin-body BEM method for studying the scattering effect of a duct numerically. An analytical formulation is derived for prediction the acoustic velocity generated by moving bodies. The acoustic velocity formulation can be used as boundary condition for thin-body BEM. Furthermore, a verification study was given based on three test cases: a pulsating sphere, a dipole source and Isom consistency test for helicopter tail rotor. The comparison is performed between analytical and numerical solution for acoustic velocity, and showed remarkable agreement. The scattering effect of duct for each case has been discussed. For the pulsating sphere, due to the scattering effect, the amplitude and directivity of SPLs are changed. For the dipole source, the amplitude only becomes greater.

References

- Brentner, K. S.; Farassat, F.** (2003): Modeling aerodynamically generated sound of helicopter rotors. *Progress in Aerospace Science*, vol.39, no.2, pp. 83-120.
- Ciskowski, R. D.; Brebbia, C. A.** (1991): *Boundary element method in acoustics*. Elsevier Science Publishing Co. Inc., New York.
- Dunn, M. H.; Tinetti, A. F.** (2008): Application of fast multipole methods to the NASA fast scattering code, *14th AIAA/CEAS Aeroacoustics Conference, AIAA*, 2008-2875.
- Dunn, M. H.; Tinetti, A. F.; Nark, D. M.** (2015): Open rotor noise prediction using the time domain formulations of Farassat. *Aeroacoustic*, vol.14, no.1-2, pp. 51-86.
- Ffowcs Williams, J. E.; Hawkings, D. L.** (1969): Sound Generated by Turbulence and Surfaces in Arbitrary Motion. *Philosophical Transactions of the Royal Society*, vol. A264, no. 1151, pp.321-342.
- Farassat, F.; Brentner, K. S.** (1988): The Uses and Abuses of the Acoustic Analogy in Helicopter Rotor Noise Prediction. *Journal of the AHS*, vol. 33, no.1, pp.29-36.
- Farassat, F.; Brentner, K. S.** (1998): Supersonic Quadruple Noise Theory for High-Speed Helicopter Rotors. *Journal of Sound and Vibration*, vol.218, no.3, pp.481-500.

- Ffowcs Williams, J. E.; Hawkins, D. L.** (1969): Sound Generated by Turbulence and Surfaces in Arbitrary Motion. *Philosophical Transactions of the Royal Society*, vol. A264, no.1151, pp. 321-342.
- Farassat, F.** (2007): Derivation of formulations 1 and 1A of Farassat. NASA, TM 214853.
- Ghorbaniasl, G.; Hirsch, C. et al.** (2015): Acoustic velocity formulation for Kirchhoff data surfaces. *Aerocoustics*, vol.14, no.1-2, pp.105-132.
- Huang, J.; Zhang, C. P.; Xiang, S. et al.** (2015): Computation of aerodynamic noise radiated from open propeller using boundary element method. *CMES-Computer Modeling in Engineering & Sciences*, vol. 108, no.5, pp. 315-330.
- Johnson, W.** (1980): *Helicopter Theory*. Princeton University Press.
- Kingan, M. J.** (2014): Advanced open rotor noise prediction. *Aeronautical Journal*, vol.118, no. 1208, pp.1125-1135.
- Kingan, M. J.; Powles, C.; Self, R.H.** (2010): Effect of centerbody scattering on advanced open rotor noise. *AIAA Journal*, vol.48, no.5, pp. 975-980.
- Lee, S.; Brentner, K.S.; Farassat, F. et al.** (2009): Analytic formulation and numerical implementation of an acoustic pressure gradient prediction. *Journal of Sound and Vibration*, vol.319, no.3-5, pp. 1200- 1221.
- Lee, S.; Brentner, K. S.; Morris, P. J.** (2010): Acoustic scattering in the time domain using an equivalent source method. *AIAA Journal*, vol.48, no.12, pp. 2772-2780.
- Mao, J. Y.; Zhang, Q. L.; Xu, C.; Qi, D. T.** (2015): Two Types of Frequency-Domain Acoustic Velocity Formulation for Rotating Thickness and Loading Sources. *AIAA Journal*, vol.53, no.3, pp.713-722.
- Mao, J. Y.; Qi, D. T.** (2009): Computation of rotating blade noise scattered by a centrifugal volute. *Proceedings of Institution of Mechanical Engineers, Part A: Journal of Power and Energy*, vol.223, no.8, pp. 965-972.
- McAlpine, A.; Astley, R.; Hii, V. et al.** (2006): Acoustic scattering by an Axially-segmented Turofan inlet duct liner at supersonic fan speeds. *Journal of Sound and Vibration*, vol. 294, no. 4-5, pp. 780-806.
- Qian, Z. Y.; Han, Z. D.; Atluri, S. N.** (2013): A fast regularized boundary integral method for practical acoustic problems. *CMES-Computer Modeling in Engineering & Sciences*, vol. 91, no.6, pp. 463-483.
- Swift, S.; Blaisdell, G.; Lyrantzis, A.** (1983): A time domain equivalent source method for acoustic scattering with coincident source and control points. *AIAA*, 2013-2017.
- Tausch, J.; Xiao, J.** (2010): A spectral boundary element method for scattering problems. *CMES-Computer Modeling in Engineering & Sciences*, vol. 58, no.3, pp. 221-245.
- Wu, T. W.** (2000): *Boundary element acoustics: fundamentals and computer codes*, WIT Press, Southampton.
- Wu, T. W.; Wan, G. C.** (1992): Numerical modeling of acoustic radiation and scattering from thin bodies using a Cauchy principal integral equation. *J. Acoust. Soc. Am.*, vol.92, pp. 2900-2906.